Numerical Investigation of Low-Frequency Longitudinal Oscillations in Hall Thrusters

IEPC-2005-120

Presented at the 29th International Electric Propulsion Conference, Princeton University
October 31 – November 4, 2005

S. Barral*
Institute of Fundamental Technological Research - PAS, 00049 Warsaw, Poland

V. Lapuerta,[†] A. Sancho[‡] and E. Ahedo[§]
Universidad Politécnica de Madrid, 28040 Madrid, Spain

The low frequency longitudinal mode of Hall thrusters is investigated using both a linear perturbation model and a non-linear model. Parametric investigations led with the linear model allow to identify the influence of some key parameters such as the magnetic field strength, the channel length and the discharge voltage. Various traveling and standing waves are identified, confined to specific regions of the thruster. The non-linear model is in turn used as a fundament for the derivation of a simplified model where only the dynamic of electrons and neutrals are described. This simplified model indicate that the breathing mode results from the interplay between a current instability and the axial motion of the ionization front.

I. Introduction

The low frequency, so called breathing mode, is the longitudinal mode that is the most systematically observed in Hall thrusters,[1] characterized by strong discharge current oscillations in the $10 - 30$ kHz band.

Most theoretical studies performed so far have consisted in deriving classical dispersion relations applied to gradient-induced instabilities,[2–4] an approach that has been shown to be mathematically inconsistent.[5] Despite the lack of consensus on a detailed theory, the essential role played by ionization has been acknowledged by a large majority of recent numerical and theoretical studies,[4, 6–8] with the sole exception of Ref. 9.

This paper reports a cooperative effort aimed at investigating the origin and properties of the low-frequency mode. A linear model, based on previous work by Ahedo et al.,[10] and a non-linear model are studied. The two models use somewhat different assumptions and highlight therefore different aspects of the oscillation mechanism, providing at the same time useful indications about the role of various hypotheses and equations on the oscillatory response of the discharge.

Section II introduces the linear perturbation model, which assumes Bohm-type diffusion while neglecting wall effects. A linear stability study is performed, showing the influence of various parameters on the stability of the mode. Section III investigates a non-linear model similar to that of Ref. 8, that is with a pressureless Ohm's law, an empirical wall interaction model and a simplified energy equation. Later on, a small subset of this model is studied with the aim to identify the main processes at play.

---

*Senior Researcher, Department of Mechanics and Physics of Fluids, sbarral@ippt.gov.pl.
†Associate Professor, Escuela Técnica Superior de Ingenieros Aeronáuticos (ETSIA), mariavictoria.lapuerta@upm.es.
‡Student, Escuela Técnica Superior de Ingenieros Aeronáuticos (ETSIA)
§Associate Professor, Escuela Técnica Superior de Ingenieros Aeronáuticos (ETSIA), eduardo.ahedo@upm.es.

II. Linear stability

A. Model formulation

This analysis is based on the models of Ahedo et al.[10] and Molina at al.[11] The time-dependent equations for the quasineutral plasma (i.e. $n_e = n_i$) are

$$\frac{\partial n_i}{\partial t} + \frac{\partial}{\partial x}(n_i v_i) = n_i(\nu_i - \nu_w), \tag{1}$$

$$\frac{\partial n_i}{\partial t} + \frac{\partial}{\partial x}(n_i v_e) = n_i(\nu_i - \nu_w), \tag{2}$$

$$\frac{\partial n_n}{\partial t} + \frac{\partial}{\partial x}(n_n v_n) = -n_i(\nu_i - \nu_w), \tag{3}$$

$$\frac{\partial}{\partial t}(m_i n_i v_i) + \frac{\partial}{\partial x}(m_i n_i v_i^2) = -en_i\frac{\partial \phi}{\partial x} + m_i n_i(\nu_i v_n - \nu_w v_i), \tag{4}$$

$$\frac{\partial}{\partial t}\left(\frac{3}{2}n_i T_e\right) + \frac{\partial}{\partial x}\left(\frac{5}{2}T_e n_i v_e\right) = n_i\left(ev_e\frac{\partial \phi}{\partial x} - \nu_i E_i' - \nu_{we}T_e\right), \tag{5}$$

$$0 = en_i\frac{\partial \phi}{\partial x} - \frac{\partial}{\partial x}(n_i T_e) - m_e n_i v_e\frac{\omega_e^2}{\nu_e}, \tag{6}$$

$$v_n = \text{const.} \tag{7}$$

Here, m_α, n_α and v_α ($\alpha = i, e, n$) are the particle mass, density and *axial* velocity of each species, respectively; ϕ is the electrical potential; T_e is the electron temperature (in energy units); $\omega_e = eB/m_e$ is the electron gyrofrequency; $\nu_i = n_n R_i(T_e)$ is the ionization frequency, with $R_i(T_e)$ the effective ionization rate; E_i' is the effective ionization energy cost per ion ($E_i' \sim 25 - 30\text{eV}$ for Xenon); ν_w represents the plasma recombination frequency at the lateral walls; $\nu_e = \alpha_{\text{ano}}\omega_e + \nu_{en} + \nu_{wm}$, is the total electron collision frequency, with contributions of anomalous diffusion, electron-neutral collisions, and wall collisionality (ν_{wm}); and ν_{we} is the effective frequency for electron energy losses. Expressions for these magnitudes can be found in Refs. 12 and 13. Electron heat conduction is omitted in this model.

The channel area A is assumed constant, thus neglecting the plume divergence. Anode and cathode are placed at the channel ends, $x_A = 0$ and $x_P = L_{ch}$. The mass flow (at the anode) is $\dot{m} = Am_i(n_n v_n + n_e v_i)$ and the discharge current is $I_d = Aen_e(v_i - v_e)$. From Eqs. (1) and (2), the discharge current is independent of x, $I_d = I_d(t)$.

We consider stationary solutions consisting of an electron-repelling anode sheath AB, of negligible thickness in the quasineutral scale ($x_B = x_A = 0$); an ion backstreaming region; the ionization region; and the acceleration region; these are regions BD, DS, and SP, respectively, in Fig. 1 below. The sheath potential drop, $\phi_{sh} = \phi_B - \phi_A$, satisfies[12]

$$\frac{e\phi_{sh}}{T_{eB}} = \frac{1}{2}\ln\frac{T_{eB}}{2\pi m_e v_{eB}^2}. \tag{8}$$

Since we are interested in small temporal fluctuations of stationary solutions, temporal derivatives may be considered as small forcing terms of the spatial problem. Then, Eqs. (1)-(7) are easily manipulated to obtain explicitly the spatial derivatives in terms of the set of plasma variables and temporal derivatives. For instance, the explicit equation for $h_e \equiv \ln n_e$ is

$$\frac{\partial h_e}{\partial x} = \frac{G}{Pv_e}, \tag{9}$$

with $P = T_e - 3m_i v_i^2/5$,

$$G = \nu_i\left[\frac{2}{5}E_i' + T_e - \frac{3}{5}m_i v_e(2v_i - v_n)\right] - m_i v_e^2\frac{\omega_e^2}{\nu_e} + \left(\frac{3}{5}m_i v_e v_i - T_e\right)\nu_\omega + T_e\nu_{we} + \frac{3}{5}m_i v_e\left(v_i\dot{h}_e - \dot{v}_i\right) + \frac{3}{5}\dot{T}_e - \frac{2}{5}T_e\dot{h}_e,$$

and dots mean time derivatives. Hence, the spatial problem presents singular points where $v_i = \pm\sqrt{5T_e/3m_i}$, that is when the isentropic Mach number for ions is equal to 1. Sonic points are regular or singular depending on $G \neq 0$ or $G = 0$, respectively.[14]

Equations (1)-(7) require seven boundary conditions distributed between points B and P. These are:[12] (i) Eq.(8); (ii) point B is sonic, $v_{iB} = -\sqrt{5T_{eB}/3m_i}$; (iii) a regular, forward sonic point (point S) exists
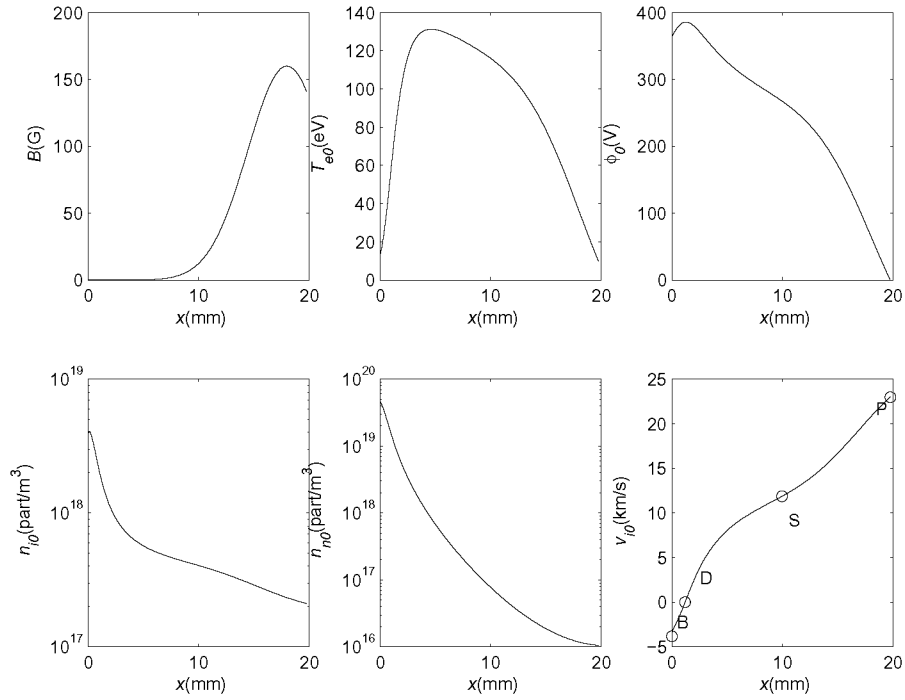
Figure 1. Steady-state solution for $V_d = 308\text{eV}$, $\dot{m} = 4.8\text{mg/s}$, L_{ch}=**19.77mm**, $B_m = 160\text{G}$, $L_m = 5\text{mm}$, x_m=**18mm**, T_{eP}=**10eV, and** v_n=**400 m/s. Points D and S correspond to zero and sonic ion velocity. Point B is the transition to the anode sheath.**

within the channel, which satisfies $G_S = 0$ and $v_{iS} = -\sqrt{5T_{eS}/3m_i}$; and (iv)-(vii) the mass flow $\dot{m}_A$, the discharge voltage $V_d = \phi_A - \phi_P$, v_n, and T_{eP} are known. The profile of the magnetic field

$$B(x) = B_m\exp\left[-(x - x_m)^2/L_m^2\right], \tag{10}$$

with B_m, x_m and L_m constant, is known too. Therefore, the plasma response in the channel depends on the following vector of control parameters

$$C = [V_d, \dot{m}_A, L_{ch}, B_m, L_m, x_m, T_{eP}, v_n]. \tag{11}$$

Alternatively, the electric power $P_d = V_d I_d$ can be imposed instead of V_d.

B.   Linear stability analysis

Let us consider now the plasma response to a small temporal perturbation on the steady-state vector of control parameters

$$C(t) = C_0 + \Re\left\{C_1\text{e}^{-\text{i}\omega t}\right\}, \quad |C_1| \ll |C_0|$$

with $\omega = \omega_{re} + \text{i}\omega_{im}$ the (complex) frequency of the perturbation mode, and subscripts 0 and 1, representing, for any variable, the steady-state and the perturbation terms, respectively. Within the linear approximation, the vector of plasma variables is of the form

$$Y(x,t) \simeq Y_0(x) + \Re\left\{Y_1(x;\omega)\exp(-\text{i}\omega t)\right\}, \quad |Y_1|/|Y_0| \sim |C_1|/|C_0|. \tag{12}$$

The linear equations for each perturbation mode in ω are obtained from the first-order terms of the expansion of Eqs. (1)-(7) and the substitution of $\partial/\partial t$ by $-\text{i}\omega$. Like the stationary equations, the perturbation equations can be singular at $P_0 = 0$ only. For instance, the equation for $h_{e1} \simeq n_{e1}/n_{e0}$ is

$$P_0 v_{e0}\frac{\partial h_{e1}}{\partial x} = G_1 - \left(\frac{v_{e1}}{v_{e0}} + \frac{P_1}{P_0}\right)G_0. \tag{13}$$
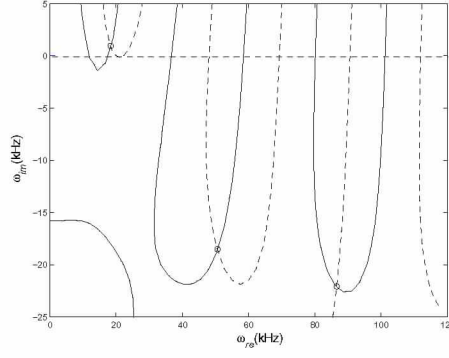
Figure 2. Solution of the dispersion relation for the case of Fig. 1. Modal frequencies are given by the intersection of $D_{re} = 0$ (solid lines) and $D_{im} = 0$ (dashed lines).

The perturbation problem requires seven boundary conditions: (i) the perturbed anode sheath potential is obtained from Eq. (8); (ii) in order to fulfill $h_{e1B} \ll h_{e0B}$, the singularity at point B for the perturbation response cannot be of higher order than for the steady response, which implies that $P_{1B} = 0$; (iii) the regularity condition at point S is

$$G_{1S} - P_{1S}\dot{G}_{0S}/\dot{P}_{0S} = 0; \tag{14}$$

and (iv)-(vii) the perturbations on control parameters are known.
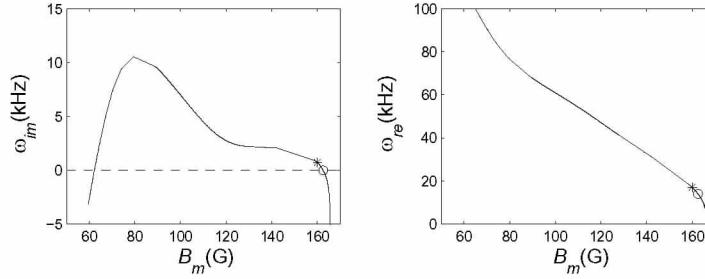
Figure 3. Influence of B_m on the first self-mode. The remaining control parameters are as in Fig. 1. Asterisk corresponds to the case of Fig. 1. The point marked with 'o' corresponds to neutral instability.

The details of the numerical integration of this perturbation problem can be found in Ref. 10. Imposing the boundary and matching conditions we obtain a matrix equation

$$M(\omega, C_0)X = B(\omega, C_0)$$

where M is a square matrix, X groups the input parameters used by the integration scheme, and B depends on the perturbations of the boundary conditions. Linear self-excited modes are solutions of the perturbation problem for $B = 0$. The frequencies of the self-excited modes are the solutions of the global dispersion relation

$$D(\omega; C_0) = 0, \qquad D \equiv \det M. \tag{15}$$

The self-excited modes are unstable if $\omega_{im} > 0$. Since $C_1 = 0$, subscript 0 is omitted hereafter on control parameters.

Figure 1 shows the steady-state solution used as starting case for the rest of computations in this section. Figure 2 plots, for that 0th order solution, the solution of the complex dispersion relation for the first three self-excited modes. The real frequencies are 17.0 kHz, 51.9 kHz, and 88.7 kHz. Only the first mode is unstable with a growing time of $\omega_i^{-1} = 0.22$ ms. Hence, this unstable mode seems to correspond to the discharge oscillations or breathing mode observed experimentally.
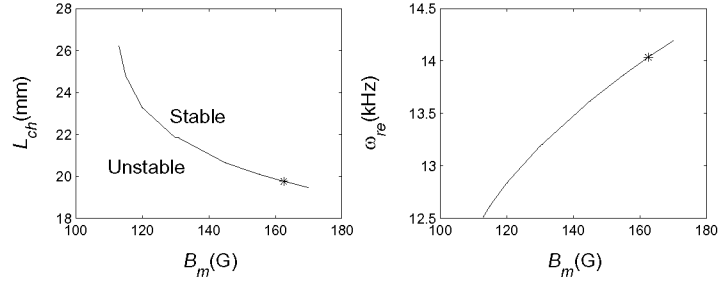
Figure 4. Stability regions in the parametric plane $B_m - L_{ch}$. The remaining control parameters are as in Fig. 1. Asterisk corresponds to neutral case of Fig. 3.
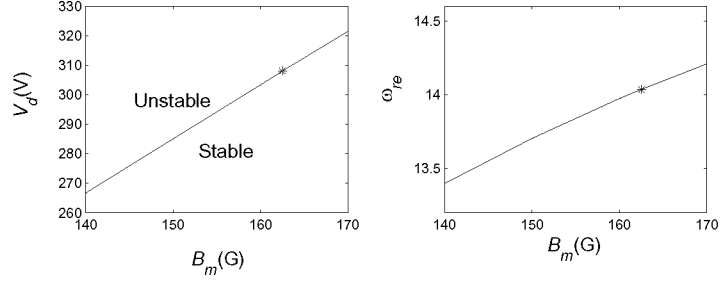
Figure 5. Stability regions in the parametric plane $B_m - V_d$. The remaining control parameters are as in Fig. 1. Asterisk corresponds to neutral case of Fig. 3.

Figures 3 to 5 display results from continuation on the control parameters with the aim of identifying the parametric threshold for stability of the above first self-mode. Starting from the case of Fig. 1, Fig. 3 displays the evolution of the frequencies of the first self-mode when the magnetic field strength is modified. The self-mode is unstable in the range $62.2G < B_m < 162.5G$. This seems to agree with the results compiled by Choueiri,[1] which show strong low-frequency discharge oscillations for an intermediate range of B_m. A similar behavior was also found by Gascon and Dudeck.[15]

Now, starting from one of the neutral stability cases of Fig. 3, figures 4 and 5 determine the stability threshold in the parametric planes B_m-V_d and $B_m - L_{ch}$. The stability region corresponds to high B_m, high L_{ch}, and low V_d. Nevertheless, notice that these trends are applicable in the threshold vicinity, since a second stability threshold, corresponding to the second neutral case of Fig. 3 must still be computed. Gascon et al.[15] found strong oscillations for high V_d.

Figure 6 shows the spatial-temporal response of one neutrally-stable mode. A three-dimensional plot is shown for n_{n1}/n_{n0}. For the rest of variables we show projections of that response on the $x - t$ plane. These plots are completed with Table 1, which yields the values of the maximum amplitudes of the plasma variables for a perturbation $I_{d1}/I_{d0} = \epsilon$ of the discharge current.

Table 1

n_{n1}/n_{n0}	5.02ϵ
n_{e1}/n_{e0}	3.27ϵ
$T_{e1}/100\text{eV}$	0.13ϵ
$\phi_1/100\text{V}$	0.17ϵ
$v_{i1}/(1000 \text{ km/s})$	0.03ϵ
v_{e1}/v_{e0}	2.24ϵ
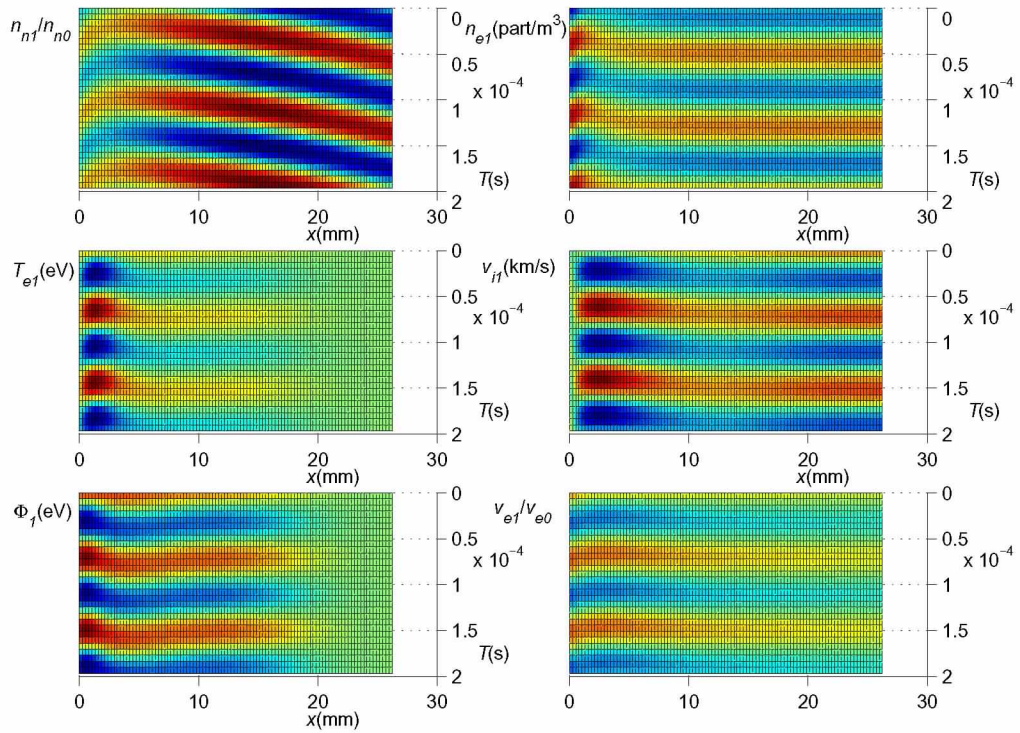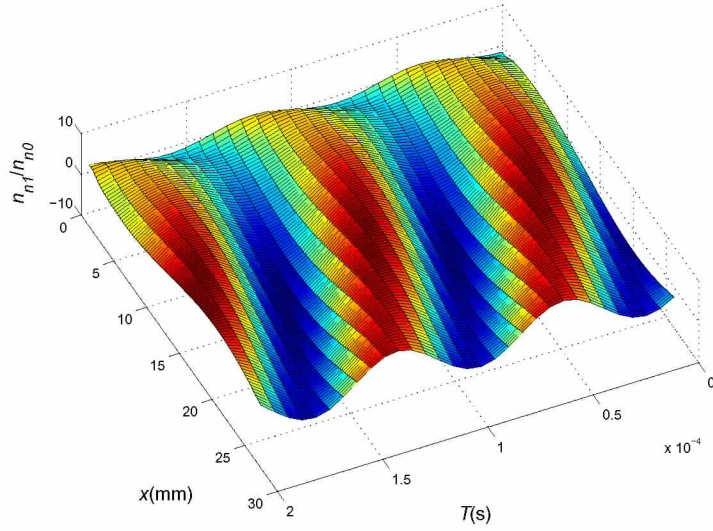
Figure 6. Spatial-temporal profiles of a neutrally-stable mode of frequency 12.5 kHz (normalized with $I_{d1}/I_{d0} = 1$). Control parameters: L_{ch}=26.22 mm, $B_m = 113$G, and the remaining parameters as in Fig. 1. In the projected profiles notice that t advances from top to bottom.

Points D ($v_{i0D} = 0$) and S(v_{i0S} sonic) are located at $x_D = 1.19$mm and $x_S = 10.34$mm. Different traveling and standing waves are observed in the figures. Neutral perturbations form a backward traveling waves, in the short ion backstreaming region, and are standing waves mounted on the stationary neutral flow, in the rest of the channel. Ion perturbations of density and velocity form: backward traveling waves in region BD; forward traveling waves in region DS, with a velocity of $200 - 250 m/s$, i.e. of the order of the velocity of neutrals, $v_n = 400 m/s$; and standing waves mounted on the stationary ion beam in region SP. These results seem to indicate that the instability is mainly developed in the back region of the channel and is associated to the traveling waves there. This would agree with computations made with the non linear model of Ref. 11, where no instability were found for *test cases* with a totally supersonic flow (from anode to cathode). This conclusion seems to be partially incompatible with the results of Sec. III, but the very different stationary profiles suggest that a direct comparison between the two models is not straightforward.
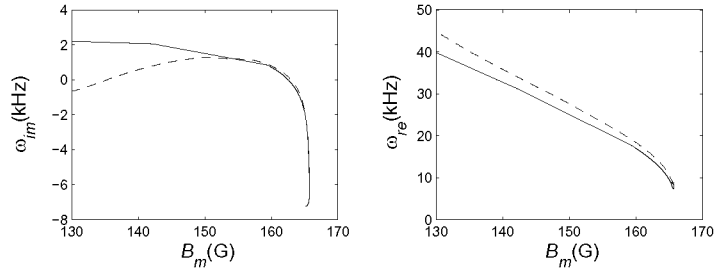
Figure 7. Influence of neglecting temporal terms in the equation for temperature. Dashed line corresponds to solutions without temporal terms in the equation for temperature. Remaining control parameters as in Fig. 1.

A common approximation in numerical simulations consists in neglecting the temporal terms in the energy equations.[8,9,16] In order to evaluate the impact of this approximation, the frequency of the first self-mode was computed for a system where the term $\partial T_e / \partial t$ was dropped. The result is compared in Fig. 7 with the case of Fig. 3. At least for this parametric region, the instability region is reduced when no temporal variations of T_e are omitted.

Finally, we note that for the case of Fig. 7, there exist two stationary solutions for the same vector of control parameters in the range $165.14\,\mathrm{G} < B_m < 165.74\,\mathrm{G}$, at least, and no stationary solution for $B_m > 165.74\,\mathrm{G}$. Mathematically, this is due to the differential problem having conditions imposed at the two boundaries. The consequence is that an oscillatory response is mandatory for $B_m > 165.74\,\mathrm{G}$. This opens a second group of oscillatory problems, yet to be investigated.

III. Non-linear model

One of the first detailed account of the breathing mode instability in a numerical model was given by Boeuf and Garrigues using a 1D hybrid description of the plasma.[8] Despite obvious shortcomings of the model, such as the use of a pressureless Ohm's law, the main features of the breathing mode were recovered. No interpretation of its results has been given, however, beyond a factual description of the motion of the oscillation front.

In this section, a reference case computed with a fluid model derived from that of Ref. 8 is investigated in a first step, and compared to the results obtained with a small subset of the initial equation system where only the dynamics of neutrals and electrons is retained. This latter, simple model, suggests in turn a physical interpretation of the ionization instability.

A. Reference model

The reference model is a translation of the hybrid model of Ref. 8 within a fully fluid formalism,

$$\frac{\partial n_n}{\partial t} + v_n \frac{\partial n_n}{\partial x} = -R_i(\mathcal{E})n_n n_e, \tag{16}$$

$$\frac{\partial n_i}{\partial t} + \frac{\partial}{\partial x}(n_i v_i) = R_i(\mathcal{E}_e)n_n n_e, \tag{17}$$

$$\frac{\partial}{\partial t}(m_i n_i v_i) + \frac{\partial}{\partial x}(m_i n_i v_i^2) = -e n_i \frac{\partial \phi}{\partial x} + R_i(\mathcal{E}_e)n_n n_e v_n, \tag{18}$$

$$\frac{\partial n_e}{\partial t} + \frac{\partial}{\partial x}(n_e v_e) = R_i(\mathcal{E}_e)n_n n_e, \tag{19}$$

$$0 = e n_e \frac{\partial \phi}{\partial x} - m_e n_e v_e \frac{\omega_e^2}{R_m n_n + \nu_{we}}, \tag{20}$$

$$\frac{\partial}{\partial t}(n_e \mathcal{E}_e) + \frac{\partial}{\partial x}(n_e v_e \mathcal{E}_e) = e n_e v_e \frac{\partial \phi}{\partial x} - E_i' R_i(\mathcal{E}_e)n_n n_e - \nu_{we}n_e \mathcal{E}_e \exp\left(-\frac{\epsilon_w}{\mathcal{E}_e}\right), \tag{21}$$

$$n_e = n_i, \tag{22}$$

$$v_n = \text{const} \tag{23}$$

where the energy of electrons $\mathcal{E}_e = \frac{3}{2}T_e$ is computed from a simplified energy equation that includes a phenomenological wall loss term with a constant electron-wall collision frequency ν_{we}. For the sake of simplicity, the pressure tensor for electrons is neglected in both the momentum (Ohm's law) and energy equations for electrons, hence the convective term in $\frac{3}{2}n_e v_e T_e$ instead of $\frac{5}{2}n_e v_e T_e$ for energy. This equation is in essence equivalent to the one of Ref. 8, except that it retains the temporal term and assumes a constant ionization cost E_i'. Note that for the test case investigated, the temporal terms of the energy equation had almost no impact on the solutions. Notwithstanding the use of a fluid description for ions, the remaining equations are strictly those of the original model.

Consistently with previous notations, point A shall denote the anode ($x = 0$) and point P the end of the domain ($x = L$). The various parameters and boundary conditions are listed below:

$$R_m = 2.5\,10^{-13}\,\text{s}^{-1}\text{m}^{-3},$$

$$R_i = \max\left(0,\ R_i^0 \frac{\frac{2}{3}\mathcal{E}_e - \epsilon_i}{\frac{2}{3}\mathcal{E}_e + E_i'}\right),$$

$$R_i^0 = 4\,10^{-13}\,\text{s}^{-1}\text{m}^{-3},$$

$$E_i' = 25\,\text{eV},$$

$$\epsilon_i = 5\,\text{eV},$$

$$\epsilon_w = 20\,\text{eV},$$

$$\nu_{we} = 0.2\,10^7\,\text{s}^{-1},$$

$$B = B_m \exp\left[-16\left(\frac{L-x}{L}\right)^2\right],$$

$$B_m = 200\,\text{G},$$

$$
\begin{aligned}
L &= 40\,\mathrm{mm}, \\
v_n &= 300\,\mathrm{m\cdot s^{-1}}, \\
[v_i]_A &= v_n \\
[\dot{m}]_A &= 5\,\mathrm{mg\cdot s^{-1}}, \\
[n_e]_A &= 10^{17}\,\mathrm{m^{-3}}, \\
[\mathcal{E}_e]_A &= 10\,\mathrm{eV}, \\
V_d = [\phi]_A - [\phi]_P &= 240\,\mathrm{V}.
\end{aligned}
$$

It can be verified that the quasi-periodic solution of this model, shown on Fig. 8, is qualitatively identical to the results of the original hybrid model for the same conditions.[8] The frequency is 18.2 kHz, versus 17.5 kHz in the hybrid model.
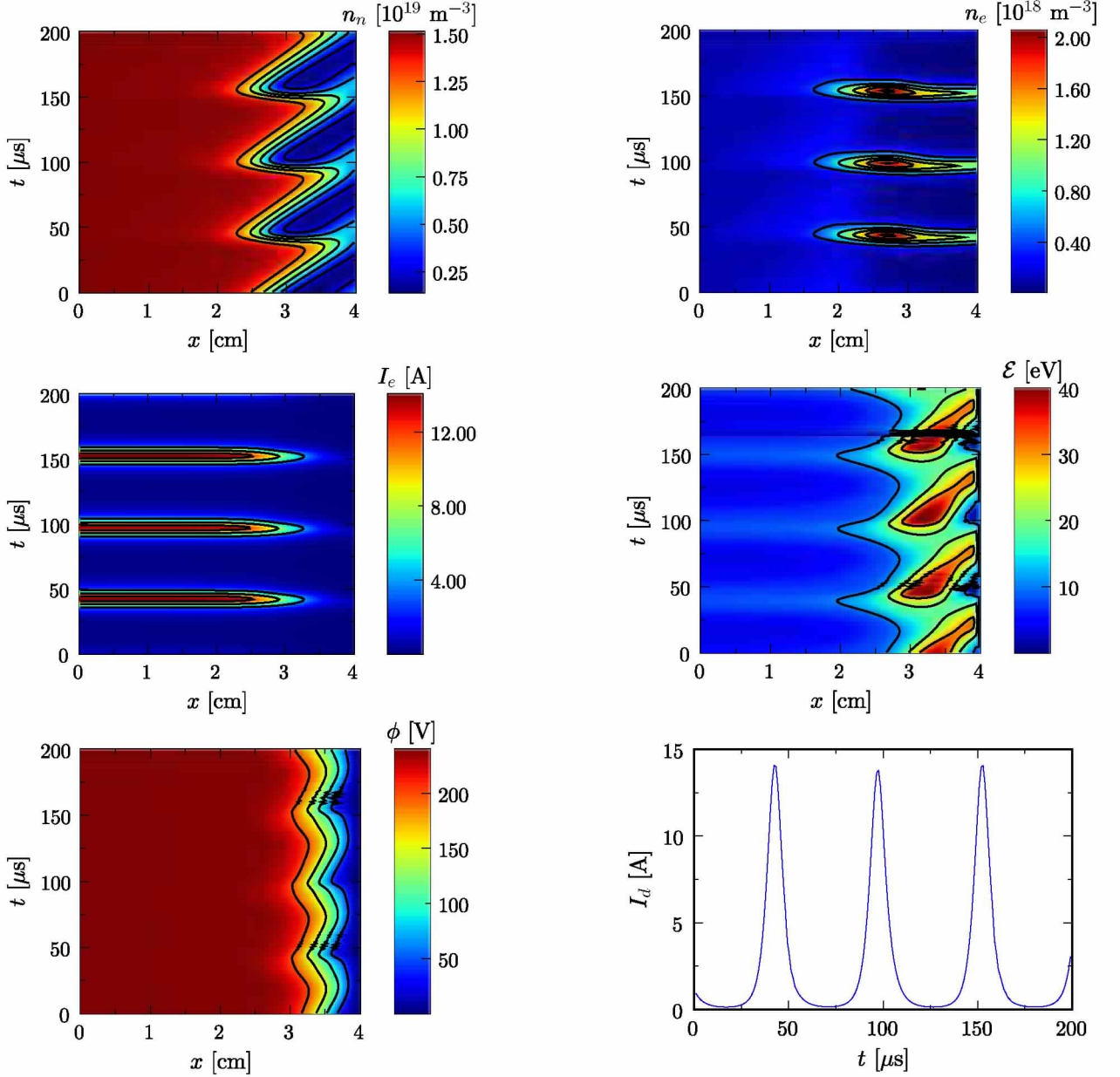
Figure 8. Quasi-periodic solution given by the reference model: density of neutrals, plasma density, electron current, electron energy, plasma potential and discharge current. $V_d = 240$ **V.**

B. Simplified model

1. Governing equations

We investigate now the following subset of the former model, where only the dynamic of neutrals and electrons is accounted for, reducing the space of variables to $(n_n, n_e, \mathcal{E})$:

$$\frac{\partial n_n}{\partial t} + v_n \frac{\partial n_n}{\partial x} = -R_i(\mathcal{E}_e)n_n n_e, \tag{24}$$

$$\frac{\partial n_e}{\partial t} + \frac{\partial}{\partial x}(n_e v_e) = R_i(\mathcal{E}_e)n_n n_e, \tag{25}$$

$$\frac{\partial}{\partial t}(n_e \mathcal{E}_e) + \frac{\partial}{\partial x}(n_e v_e \mathcal{E}_e) = en_e v_e \frac{\partial \phi}{\partial x} - E'_i R_i(\mathcal{E}_e)n_n n_e - \nu_{we} n_e \mathcal{E}_e \exp\left(-\frac{\epsilon_w}{\mathcal{E}_e}\right), \tag{26}$$

assuming time-independent profiles of the potential and electron axial velocity:

$$\phi = \bar{\phi}(x)$$
$$v_e = \bar{v}_e(x)$$

where $\bar{\phi}$ and $\bar{v}_e$ are the stationary solutions of the model of Sec. A. The assumption on ϕ is justified in view of the small displacement of equipotential lines with time, in comparison to the motion of the ionization front. Assuming that v_e is stationary is admittedly a strong assumption. As will be seen, however, this approximation turns out not to be so crucial for reproducing the breathing mode, because the oscillation mechanism appears mostly related to mass and energy transfers, while momentum equations only set the convection velocity. The oscillation of the velocity of electrons has thus mostly an effect on the transit times than on the magnitude of the convected mass and energy fluxes.

2. Boundary conditions

In order to close the system, we neglect the ion flow at anode (point A), so that the discharge current is simply given by

$$I_d = -eA[n_e v_e]_A. \tag{27}$$

Additionally, the quasineutrality assumption allows us to write the plasma density in the exit plane as

$$[n_e]_P = \frac{I_d}{eA[v_i - v_e]_P}, \tag{28}$$

where v_e is known (imposed), while the ion exhaust velocity can be reasonably approximated by

$$[v_i]_P \approx \sqrt{\frac{2eV_d}{m_i}}. \tag{29}$$

Combining Eqs (27-29), one gets:

$$[n_e v_e]_P = \frac{1}{\bar{\alpha}_e + 1}[n_e v_e]_A, \tag{30}$$

where

$$\bar{\alpha}_e = \frac{[n_e v_e]_A - [n_e v_e]_P}{[n_e v_e]_P} = -\frac{[n_e v_i]_P}{[n_e v_e]_P} \approx -\frac{\sqrt{\frac{2eV_d}{m_i}}}{[v_e]_P}, \tag{31}$$

is a constant representing the number of electrons (or ions) produced inside the channel for each electron introduced at point P in the stationary case. It will be later on referred to as the stationary electron multiplication ratio. Eq. (30) is obviously only an approximation resulting mainly from the fact that we consider v_e as stationary, but it does captures an essential mechanism of the Hall thruster discharge, inasmuch

as the magnitude of the electron current inside the low electron mobility region (high magnetic field) can be shown to be tightly coupled to that of the discharge current.

Summarizing, the boundary conditions of the simplified model read

$$[n_n v_n]_A = \frac{\dot{m}_n}{m_n A}, \tag{32}$$

$$[n_e v_{ex}]_P = \frac{1}{\bar{\alpha}_e + 1} [n_e v_{ex}]_A, \tag{33}$$

$$[\mathcal{E}_e]_P = \mathcal{E}_e^P. \tag{34}$$
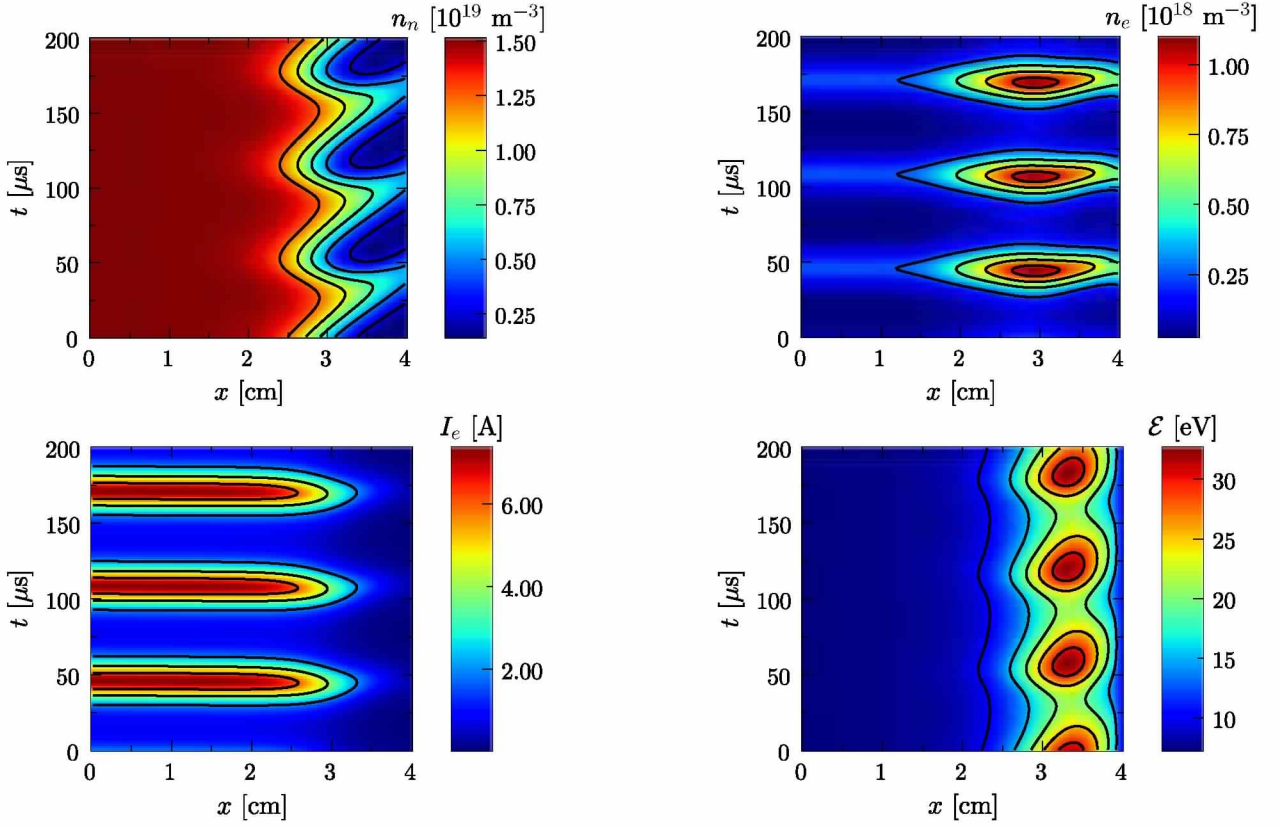
Figure 9. **Simplified model with stationary profiles of $\phi(x)$ and $v_e(x)$: density of neutrals, plasma density, electron current and energy of electrons.** $V_d = 240\,\mathbf{V}.$

3. Results and interpretation

The results obtained in the same conditions as previously with the simplified model are shown on Fig. 9. Despite some quantitative differences regarding the amplitude of oscillations and, to a lesser extend, their frequency (16.1 kHz instead of 18.2 kHz earlier), the main features of the instability appear qualitatively unchanged. The mechanism at play would therefore involve an interaction between neutrals and electrons,[4,7] rather than an interaction between ions and neutrals.[6] The interpretation of the breathing mode based on an electric field instability[9] appears in any case extremely difficult to justify in the light of these results.

Phenomenological insight into the ionization instability can be obtained by analyzing the ionization process in the stationary case. Leaving aside wall interactions, Eq. (26) raises the total ion production rate,

$$\frac{\dot{m}_i}{m_i} = A \int_A^P R_i(\mathcal{E}_e) n_n n_e dx = \frac{1}{E_i'} \left\{ A \int_A^P e n_e v_e \frac{\partial \phi}{\partial x} dx - A [n_e v_e \mathcal{E}_e]_A^P \right\}. \tag{35}$$

The total energy flux of electrons $A n_e v_e \mathcal{E}_e$ is typically small at point P, but amounts to $I_d \mathcal{E}_e / e$ at point A. $\mathcal{E}_e$ at point A is usually of the order of the ionization threshold energy ϵ_i, which is to be compared to the total

ionization power, typically of order $I_d E_i'/e$. Assuming that $\epsilon_i \ll E_i'$, we may thus also neglect the electron energy flux $A n_e v_e \mathcal{E}_e$ at point A in the total energy balance to obtain the following approximate law,

$$\frac{\dot{m}_i}{m_i} \approx \frac{eA}{E_i'} \int_A^P n_e v_e \frac{\partial \phi}{\partial x} dx. \tag{36}$$

Physically, this approximation consists in neglecting the energy of electrons introduced by the cathode and the energy deposited by electrons on the anode.

Eq. (36) makes it clear that ionization is enhanced when the magnitude of $n_e v_e$ is already large where $-\partial \phi / \partial x$ is large, that is, if the ionization zone is located in a high electric field region. Indeed, those electrons resulting from ionization can then gain additional energy from the electric field, allowing in turn more neutrals to be ionized. Such an increase in ionization efficiency is therefore not strictly a consequence of a greater heating of each single electron, but rather proceeds from the fact that more secondary electrons are heated. It is interesting to note that the supplemental electron Joule heating is actually drawn at the expense of ion acceleration: the potential drop seen by ions is indeed lower when ionization takes place inside the high electric field region. The approximation of Eq. (29) remains qualitatively valid, however, since the ionization power involved is only of the order of $I_d E_i'/e$ while the ion acceleration power is of the order of the total power, $I_d V_d$.

Having shown that the ionization efficiency strongly depends upon the location of the ionization front, let us now examine the electron avalanche process in more details. Obviously, the total instantaneous ion production rate is equal to the total electron production rate, that is,

$$\frac{\dot{m}_e}{m_e} = A \int_A^P R_i(\mathcal{E}_e) n_n n_e dx \tag{37}$$

The instantaneous electron multiplication ratio, that is the number of electrons produced at a given instant for each electron introduced at point P, is in turn given by

$$\alpha_e = \frac{\dot{m}_e/m_e}{A[n_e v_e]_P} = \frac{\int_A^P R_i(\mathcal{E}_e) n_n n_e dx}{[n_e v_e]_P}. \tag{38}$$

Therefore, if α_e comes to exceed the stationary value $\bar{\alpha}_e$, the current collected at the anode (point A) grows above the stationary value and induces via Eq. (30) a growth of the electron current at point P that further increases ionization and the current collected at point A. In effect, the multiplication of electrons inside the channel, together with Eq. (30), constitutes a closed loop with positive feedback, the amplification of which is $\frac{\alpha_e+1}{\bar{\alpha}_e+1}$. For $\alpha_e > \bar{\alpha}_e$, an electron avalanche occurs that results in a backward motion of the front of neutrals, thus displacing the ionization zone toward the region of low electric field. Eventually, α_e drops below $\bar{\alpha}_e$, ionization rapidly slows down and the repletion of neutrals resumes until α_e crosses the threshold again. The positive feedback instability is confirmed by synchronous plots of I_d and α_e on Fig. 10.
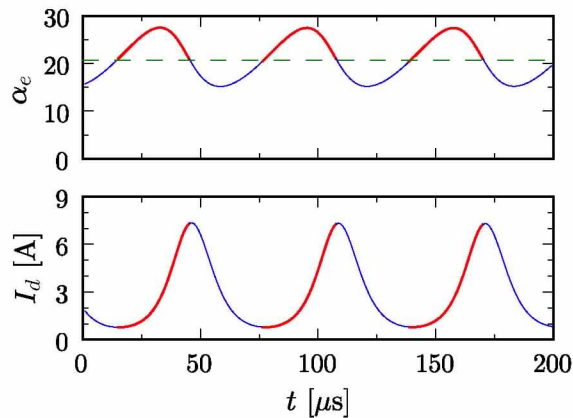
Figure 10. Electron multiplication ratio α_e and discharge current I_d in the simplified model. It can be seen that the slope of the discharge current is directly influenced by the crossing of the stationary multiplication ratio $\bar{\alpha}_e$ (dashed line).

The process involves therefore two time scales: (i) the time delay incurred by the transit of electrons to close the feedback loop, *i.e.* to transmit information from the cathode (point P) to the anode (point A) and (ii) the transit-time of neutrals, which determines the time needed to replete the channel. On the one hand, the predator-prey mechanism suggested earlier[6] appears quite insightful if applied to electrons and neutrals, at least from a qualitative point of view. On the other hand, the instability is obviously deeply affected by the features of the positive feedback loop which in turn depend on the axial distribution of the various plasma parameters such as the electric field, making a classical predator-prey model inapplicable.

IV.   Conclusion

The results reported here are preliminary, but hopefully open the way for a better understanding of the breathing mode.

The linear study brings the following provisional conclusions concerning the parametric behavior and the main characteristics of the instability:

- The stability character of the self-modes depends on the strength of the magnetic field, with unstable waves existing only for an intermediate range of B_m, which seems in qualitative agreement with some experiments.

- The channel length discharge voltage affect the stability thresholds.

- Temporal terms in the energy equation for temperature should not be neglected for low magnetic fields, since they are then of dominant order and increase the instability region.

- Self modes present a different behavior in the ion-backstreaming, ionization and acceleration regions. Different traveling and standing waves coexist.

- Multiple stationary solutions exist for certain operation conditions, which unveils another class of oscillatory solutions.

The non-linear model highlights in turn some key processes of the breathing mode, namely:

- The oscillation directly involves only electrons and neutrals, consistently with the conjecture formulated by some authors,[4,7] with a mechanism reminiscent of that of predator-prey systems.

- The destabilizing mechanism results from a positive feedback current loop, whereas the ionization-induced multiplication of electrons flowing from the low mobility region generates, with some delay, an electron current at anode ($\approx$discharge current) which itself synchronously sets the electron current flowing in the low mobility region.

- The stabilizing mechanism is related to the displacement of the front of neutrals, which tends to displace the ionization zone back or forth such as to bring the electron multiplication ratio to values that oppose the effect of the current instability

It remains unclear, however, how the conclusions of the linear study apply to the non-linear model. Conversely, the mechanism suggested by the non-linear model still needs to be unambiguously identified within the linear model. The resolution of these issues will be the object of future works, which will hopefully eventually lead to the formulation of a simple analytical model of the breathing mode.

Acknowledgments

References

[1] E. Y. Choueiri. Plasma oscillations in Hall thrusters. *Phys. Plasmas*, 8:1411, 2001.

[2] Yu. B. Esipchuk and G. N. Tilinin. Drift instability in a Hall-current plasma accelerator. *Sov. Phys. Tech. Phys.*, 21:417, 1976.

[3] V. I. Baranov, Yu. S. Nazarenko, V. A. Petrosov, A. I. Vasin, and Yu. M. Yashnov. New conception of oscillation mechanisms in the accelerators with closed drift of electrons. In *Proc. 24th International Electric Propulsion Conference*, number 95-044, Moscow, 1995. The Electric Rocket Propulsion Society, Worthington, OH.

[4] N. Yamamoto, K. Komurasaki, and Y. Arakawa. Condition of stable operation in a Hall thruster. In *Proc. 28th International Electric Propulsion Conference*, number 03-086, Toulouse (France), 2003. The Electric Rocket Propulsion Society, Worthington, OH.

[5] S. Barral, K. Makowski, Z. Peradzyński, and M. Dudeck. Transit-time instability in Hall thrusters. *Phys. Plasmas*, 12(073504), 2005.

[6] J. M. Fife, M. Martinez-Sanchez, and J. Szabo. A numerical study of low-frequency discharge oscillations in Hall thrusters. In *Proc. 33rd AIAA Joint Propulsion Conference*, number 97-3051, Seattle, 1997. American Institute of Aeronautics and Astronautics, Washington, D.C.

[7] V. I. Baranov, Yu. S. Nazarenko, V. A. Petrosov, A. I. Vasin, and Yu. M. Yashnov. Theory of oscillations and conductivity for Hall thrusters. In *Proc. 32nd AIAA Joint Propulsion Conference*, number 96-3192, Lake Buena Vista, 1996. American Institute of Aeronautics and Astronautics, Washington, D.C.

[8] J.-P. Boeuf and L. Garrigues. Low frequency oscillations in a stationary plasma thruster. *J. Appl. Phys.*, 84:3541, 1998.

[9] S. Chable and F. Rogier. Plasma oscillations in Hall thrusters. *Phys. Plasmas*, 12(033504), 2005.

[10] E. Ahedo, P. Martinez, and M. Martinez-Sanchez. Steady and linearly-unsteady analysis of a Hall thruster with an internal sonic point. In *Proc. 36th AIAA Joint Propulsion Conference*, number 2000-3655, Huntsville, 2000. American Institute of Aeronautics and Astronautics, Washington, D.C.

[11] A. Molina, V. Lapuerta, and E. Ahedo. Time-dependent model of the Hall thruster discharge. In *Proc. 39th AIAA Joint Propulsion Conference*, number 2003-4856, Huntsville, 2003. American Institute of Aeronautics and Astronautics, Washington, D.C.

[12] E. Ahedo, P. Martinez-Cerezo, and M. Martinez-Sanchez. One-dimensional model of the plasma flow in a Hall thruster. *Phys. Plasmas*, 8:3058, 2001.

[13] E. Ahedo, J. M. Gallardo, and M. Martinez-Sanchez. Effects of the radial plasma-wall interaction on the Hall thruster discharge. *Phys. Plasmas*, 10:3397, 2003.

[14] E. Ahedo and M. Martinez-Sanchez. One-dimensional plasma structure in Hall thruster. In *Proc. 34th AIAA Joint Propulsion Conference*, number 98-8788, Cleveland, 1998. American Institute of Aeronautics and Astronautics, Washington, D.C.

[15] N. Gascon, M. Dudeck, and S. Barral. Wall material effects in stationary plasma thrusters. I. Parametric studies of an SPT-100. *Phys. Plasmas*, 10:4123, 2003.

[16] S. Barral, K. Makowski, Z. Peradzyński, N. Gascon, and M. Dudeck. Wall material effects in stationary plasma thrusters. II. Near-wall and in-wall conductivity. *Phys. Plasmas*, 10:4137, 2003.